Supporting Information

Polyethylene fibers containing directional microchannels for passive radiative cooling

Mengxia Sun, Fei Peng, Shanshan Xu, Xianhu Liu, Kun Dai, Guoqiang Zheng, Chuntai Liu and Changyu Shen*

School of Materials Science and Engineering, Key Laboratory of Material Processing and Mold (Ministry of Education), National Engineering Research Center for Advanced Polymer Processing Technology, Zhengzhou University, Zhengzhou 450000, PR China

E-mail address: gqzheng@zzu.edu.cn (G. Zheng)

Note S1 Calculation of shear rate

The shear rate of PFCDM can be calculated by:

$$\gamma = \frac{6q}{\pi R^3} \tag{1}$$

where R is inner diameter of die exit and q is volume rate of the extruder during extrusion. Herein, q and R were respectively 15 cm^3/min, 3 mm. Therefore, γ is 17.8 rad/s.

Note S2 Porosity measurement

Porosity of PFCDM was estimated via the ethanol saturation method. First, the mass and volume of PFCDM were measured, respectively denoted as $W_1$and V_1, then the measured PFCDM was placed in anhydrous ethanol. After PFCDM fully absorbed anhydrous ethanol to equilibrium, PFCDM was taken out and the residual ethanol on the surface of PFCDM was wiped with filter paper. Then PFCDM was weighed again (recorded as W_2). Finally, the porosity was calculated by the following equation：

$$porosity = \frac{W_2 - W_1}{V_1 \times \rho} \times 100\% \tag{2}$$

where ρ is the ethanol density. The final porosity was obtained by measuring 10 samples to obtain the mean and standard deviation.

Note S3 Calculation of cooling power

$$P_{cooling} = P_{rad}(T) - P_{sun} - P_{atm}(T_{amb}) - P_{non-rad} \tag{3}$$

$$P_{rad}(T) = 2\pi \int_0^{2\pi} d\theta \sin\theta \cos\theta \int_{2.5\mu m}^{25\mu m} I_{BB}(T,\lambda)\varepsilon(\lambda,\theta)d\lambda \tag{4}$$

$$I_{BB}(T,\lambda) = \frac{2hc^2}{\lambda^5} \frac{1}{e^{hc/\lambda K_B T} - 1} \tag{5}$$

where here $\varepsilon(\lambda,\theta)$ is the spectral and angular emissivity of the cooler. h is Planck's constant, K_B is Boltzmann constant, and c is the speed of light.

$$P_{sun} = \int_{0.3\mu m}^{2.5\mu m} I_{solar}(\lambda)\varepsilon(\lambda,0)d\lambda \tag{6}$$

$$P_{atm}(T_{amb}) = 2\pi \int_{0}^{\frac{\pi}{2}} d\theta \sin\theta\cos\theta \int_{2.5\mu m}^{25\mu m} I_{BB}(T,\lambda)\varepsilon(\lambda,\theta)\varepsilon_{atm}(\lambda,\theta)d\lambda \tag{7}$$

$\varepsilon_{atm}(\lambda,\theta)$ is the spectral and angular emissivity of the atmosphere, which can be defined as:

$$\varepsilon_{atm}(\lambda,\theta) = 1 - t(\lambda)^{\frac{1}{\cos\theta}} \tag{8}$$

where $t(\lambda)$ is the atmospheric transmittance in the zenith direction, which can be obtained by MODTRAN of Mid-Latitude Summer Atmosphere Model (MODTRAN (spectral.com)).

$$P_{non-rad} = h_c(T_{amb} - T) \tag{9}$$

where h_c is the coefficient of the non-radiative heat.

Note S4 Comparison of wearable PRC fabrics and PRC aerogels for energy saving buildings

(1) PRC fabrics and PRC aerogels have high solar reflectivity in order to avoid heating from solar radiation. In addition, both PRC fabrics and PRC aerogels improve thermal insulation by introducing porous structure. Therefore, both PRC fabrics and PRC aerogels have radiative cooling properties.

(2) Although both PRC fabrics and PRC aerogels have microporous structures, PRC fabrics have smaller pore sizes than PRC aerogels. On the one hand, this work achieves high reflectivity through microstructures with similar wavelength size to ultraviolet, mid-infrared and visible light[1], so the diameter of pore is smaller than that of PRC aerogels. On the other hand, because PRC fabric is used in the field of human wear, it is quite different from PRC aerogels application scenarios. Therefore, the overall size

of PRC fabric is smaller than PRC aerogel, and it also takes into account the functions of air permeability, softness and comfort to ensure the experience of the wearer while ensuring the radiative cooling performance.

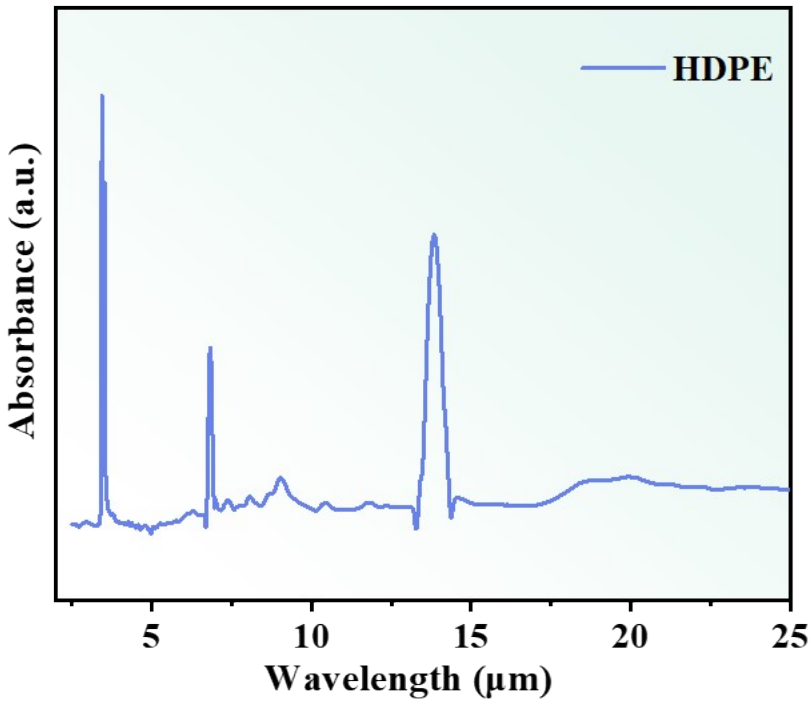

Fig. S1 The infrared result shows that the absorption vibration peaks are far away from 8-13 μm. Therefore, HDPE provides a strong mid-infrared emissivity at atmospheric window.

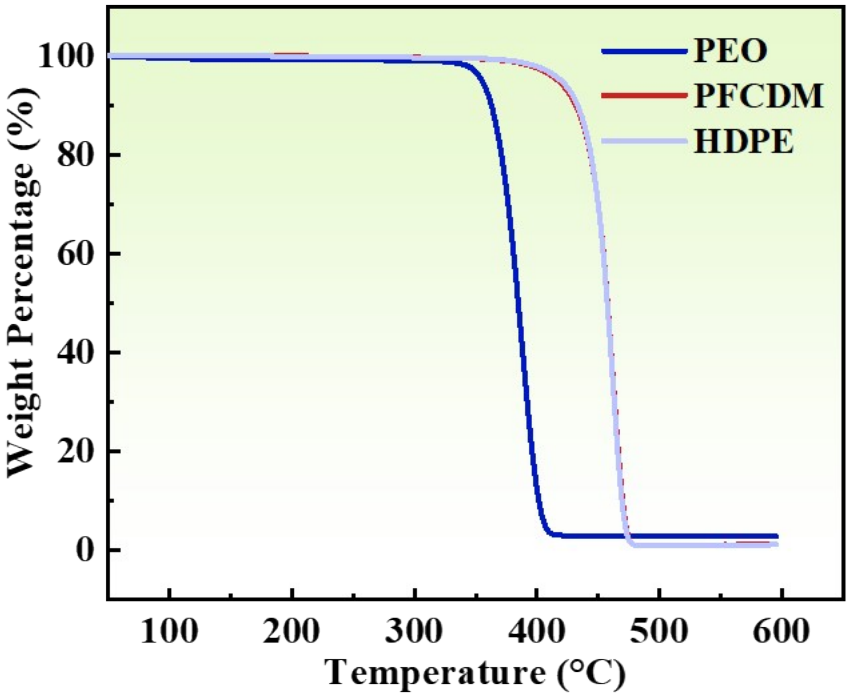

Fig. S2 TG results show that PEO in PFCDM has been leached.

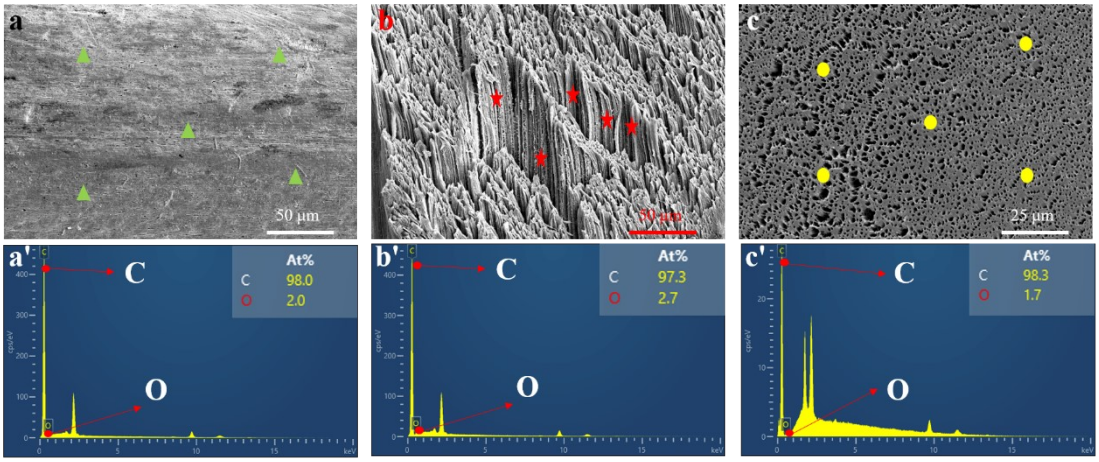

Fig. S3 Oxygen content measure results of PFCDM. The oxygen content of PFCDM (a) surface, (b) longitudinal section and (c) cross section was measured by point scanning mode.

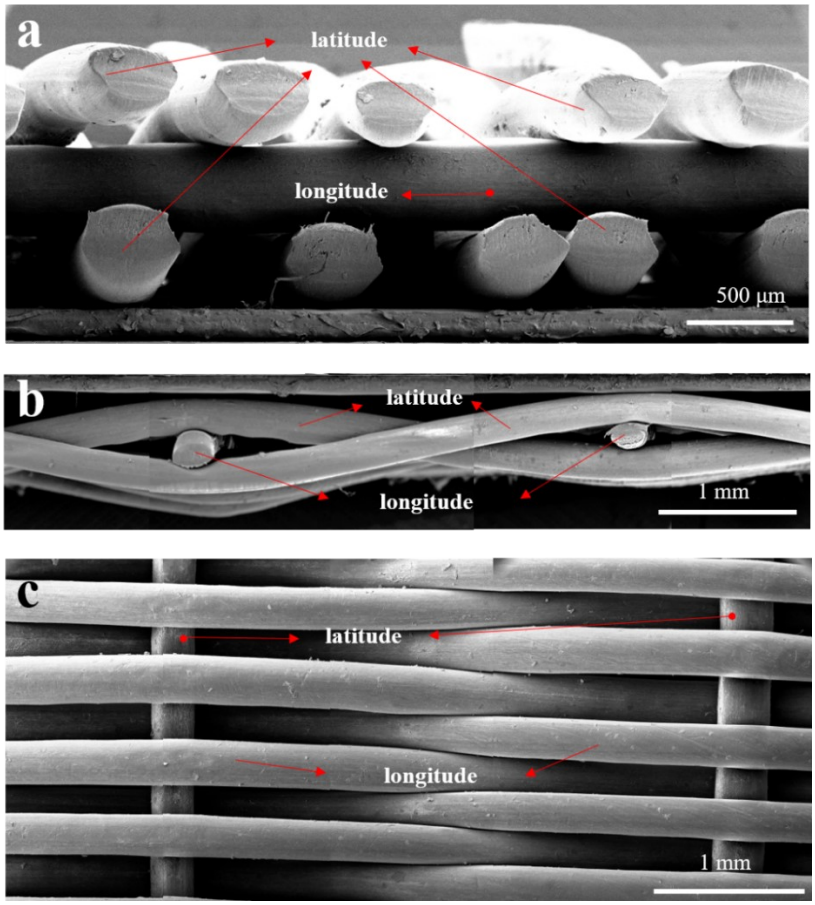

Fig S4 Morphology of PFCDM fabric. (a) Cross section parallel to the longtitude. (b) Cross section parallel to the latitude. (c) Surface of PFCDM fabric.

The warp and weft weaving method was used in this work, and the warp lines were about 3.5 mm apart as shown in Fig. S4.

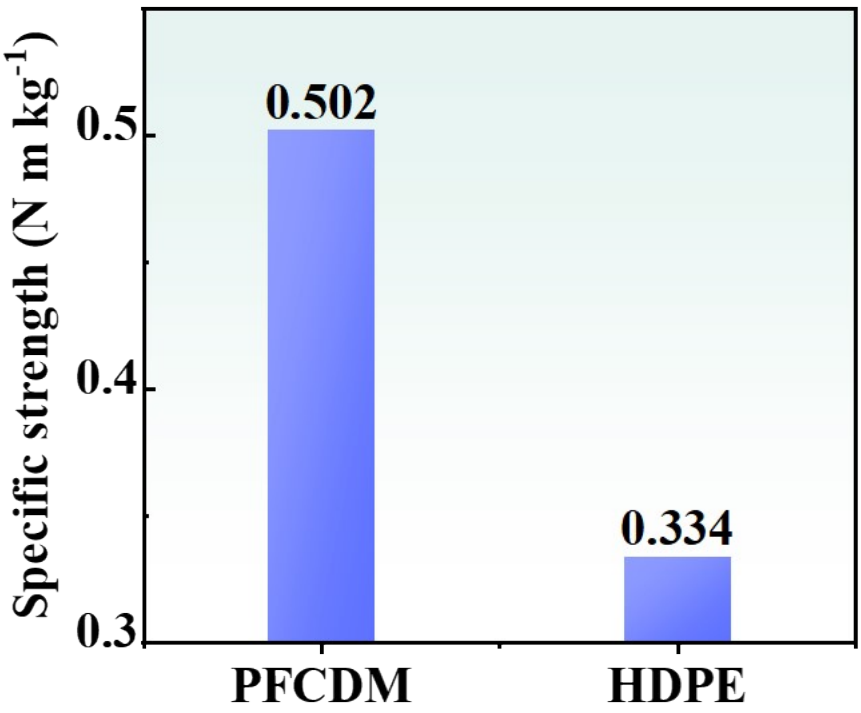

Fig. S5 The specific strength of PFCDM is 0.502 N m kg^{-1} and that of HDPE is 0.334 N m kg^{-1}

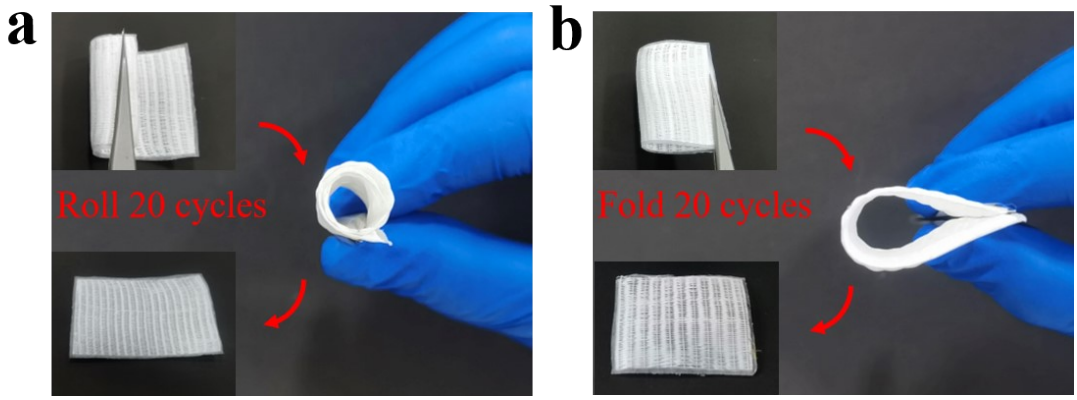

Fig. S6 PFCDM fabric can maintain its original shape after being a) rolled and b) folded 20 times

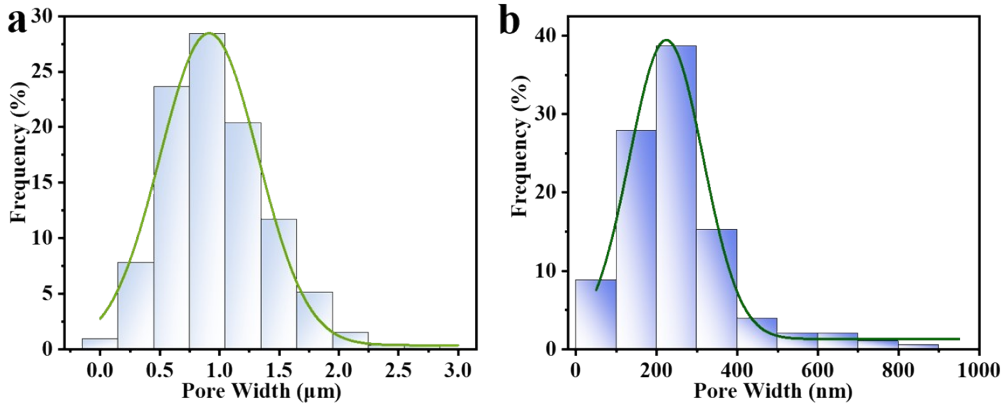

Fig. S7 The diameter distribution of a) microchannels and b) microgrooves.

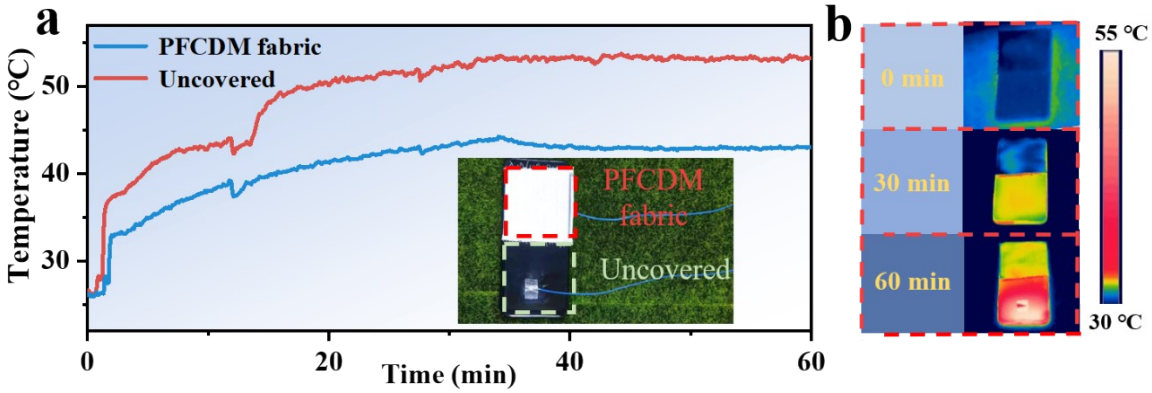

Fig. S8 a) Measured temperature of the phones uncovered as well as covered with PFCDM fabric. b) Infrared images of aforementioned phone were taken every 30 minutes.

During the test, a common software was running in the mobile phone to simulate normal use. The results show that PFCDM fabric can not only prevent the phone from overheating but also prevent wearer from feeling the heat of phone.

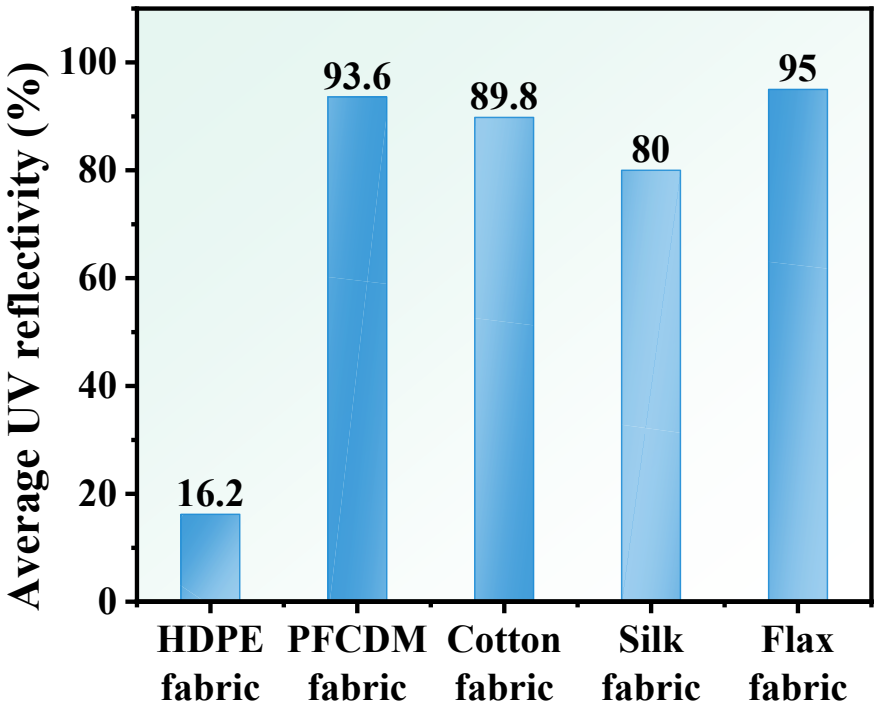

Fig S9 Average UV reflectivity of different fabrics.

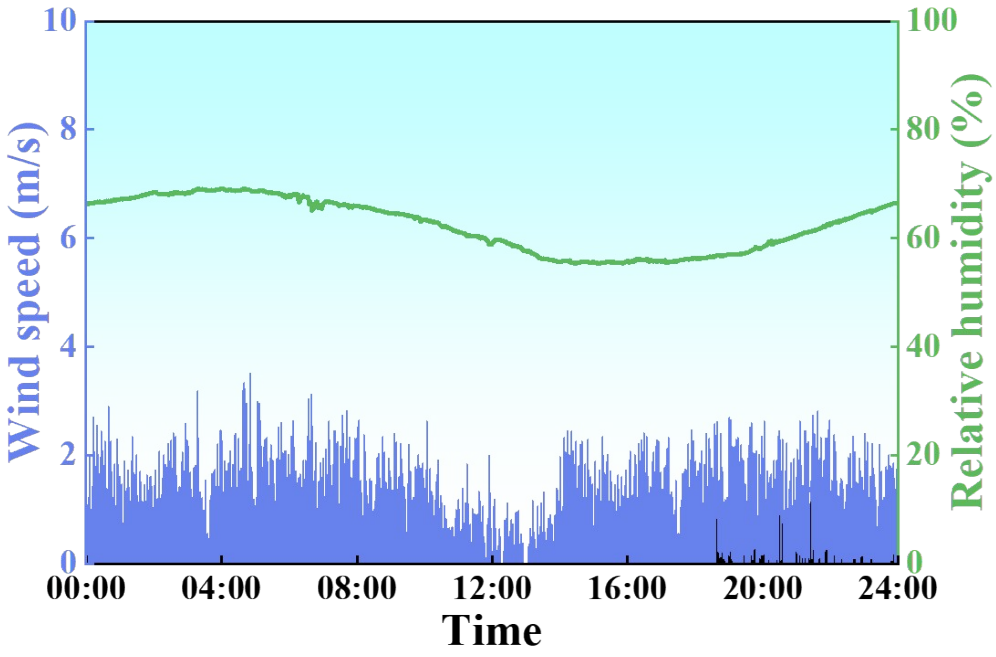

Fig. S10 Corresponding wind speed and relative humidity when performing outdoor PRC measurement.

Supporting Videos

Video S1 Remarkable air permeability and hydrophobicity of PFCDM fabric

Video S2 Application for human radiative cooling

Video S3.1 Self-cleaning property of fabrics contaminated by powders

Video S3.2 Self-cleaning property of fabrics contaminated by droplets

According to Table S1, PFCDM fabric has the greatest temperature drop and outstanding cooling power compared to reported PRC fabric work. It is worth noting that we further compared PFCDM fabric with the reported PRC materials, PFCDM fabric has excellent radiative cooling performance, but also has good air permeability and self-cleaning performance (Table S2). Therefore, PFCDM fabrics have remarkable innovation and excellent performance in PRC fabrics.

Table S1 Comparison of PFCDM fabric with previously reported PRC fabric work

Materials	Year	Temperature drop (◦C)	Cooling power (W m^{-2})
PVDF/TEOS[2]	2020	6	100
PMMA/$CsPbBr_xI_{3-x}$ quantum dots[3]	2023	4	---
PVDF[4]	2020	17.7	---
CS/SiO_2[5]	2023	11.2	103.3
Nano-Ag/PE[6]	2017	7.1	---
PVDF/PE[7]	2020	6.5	72.78
HIRC[8]	2022	5.1	104
PVDF-HFP/PPy	2022	4.5	83
PTFE[9]	2021	4.8	50
HDPE (this work)	2023	27.71	104.285

Table S2 Comparison of PFCDM fabric with previously reported work[10-13]

Material and structure	Cooling performance (other performance)	Experiment condition	Application	Year
Seven layers of HfO_2 and SiO_2	4.9 ℃ below ambient air temperature and cooling power of 40.1 W m^{-2}	850 W m^{-2} average solar irradiance	Building exterior	2014
A multilayered structure consisting of porous PTFE and a cermet-based spectrally selective absorber	Provide tunable optical properties, allowing a highly reversible change in solar transmittance of 0.62. Leading to annual cooling and heating savings of around 77% and 27%, respectively	Under direct solar irradiance	Building exterior	2022
50 mm-thick polymer glass bead hybrid organic inorganic film and a 200 nm-thick Ag thin film layers	Cool water to 10.6 ℃ below ambient and an average cooling power of 607 W m^{-2} at noon (12–2 p.m.)	952 W m^{-2} average solar irradiance at 26.5 L $(h\ m^2)^{-1}$ volumetric flow rate	Water-based radiative cooling for building	2019
Five alternating layers of a-Si:H and SiO2 multilayers coated with 50 μm-thick PDMS layer	Average 5.2 ℃ temperature reduction of an inner temperature compares to the transparent selective emitter that transmits most of the incoming solar irradiance under direct sunlight	550 W m^{-2} of peak solar irradiance	Enclosure	2021
PDMS layer, Ag layer, and 500 mm-thick micro-patterned quartz layers coated with 10 μm of PDMS from top to bottom	Lowered the temperature of a radiative object inside an enclosure by an average 4 ℃ compared to a conventional radiative cooler, which is composed of an aluminum plate coated with ~100 μm thick PDMS	810 W m^{-2} average solar power and average humidity of ~44%	Enclosure	2020
Nano polyethylene	2.7 and 2 ℃ lower skin temperature when covered with nanoPE cloth and with processed nanoPE cloth than when covered with cotton	Skin simulator	Textile	2016
PTFE/TiO_2 embedded PLA fibers	5, 6.8, 7, 5.8, and 10.2 ℃ lower than that of the cotton, spandex, chiffon, linen, and bare skin simulator	~620 W m^{-2} of peak solar irradiance	Textile	2021
Polyethylene fibers containing directional microchannels (this work*)	Skin covered by PFCDM fabric is 27.71 ℃ cooler than bare skin	~892 W m^{-2} of peak solar irradiance	Textile	2023
Porous SEBS	~7 ℃ cooling than non-porous SEBS covered skin	~840 W m^{-2} of peak solar irradiance	Wearable devices	2020
Porous PMMA/SEBS bi-layer	~7 ℃ cooling than black elastomer covered skin after 7 min exposure to sunlight	~820 W m^{-2} of solar intensity, 18 ℃ of ambient temperature	Wearable Devices	2021

Two dimensional SIO_2 micro grating	Average 6 ℃ cooling, leading to absolute increase of 2% in open-circuit voltage for InGaP/GaAs/Ge multi-junction solar cell	989 W m^{-2} of peak solar intensity and a clear sky	Solar cell	2021
Soda-lime glass wafer	Achieving 5 ℃ to 36 ℃ temperature drop and an 8% to 27% relative increase of open-circuit voltage for a GaSb solar cell	5 to 6 W of average heat load on the solar cell	Solar cell	2020
A glass-polymer hybrid film	Output voltage of ~40 mV cm^{-2} and an output power of ~10 nW cm^{-2}	~500 W m^{-2} of solar irradiance and ~25 ℃ of ambient temperature	TEG	2021
Black paint coated aluminum disk	Cooling 4–5 ℃ under ambient air (cold side), experimentally 25 mWm^{-2} of power generation	Nighttime outdoor condition	TEG	2019
The structure consists of layers of PDMS and Ag on an aluminum (Al) substrate, with a thickness of 100 μm, 150 nm, and 1 mm	(Condensation rate) below 10 ℃ of ambient temperature and condensing ~8.5 mL per day	800 W m^{-2} of peak solar intensity and all the devices were tilted ~15° toward the west to reduce absorption of solar radiation	Dew harvesting	2021
A multi-layer of PDMS 100 μm on 500 μm of glass substrate. The backside of the substrate is coated with 140 nm of Ag and 1 nm of chromium	(Condensation rate) 52 g m^{-2} h^{-1} of dew mass flux is obtained over a period of nearly 3 h	200 W m^{-2} of solar irradiance and at a mean RH of 96% in August	Dew harvesting	2021
$W_xV_{1-x}O_2/BaF_2$ 2D grating on Ag	Emissivity from 0.2 for ambient temperatures lower than 15 ℃ to 0.90 for temperature above 30 ℃	Under direct solar irradiance	Self-adaptive radiative thermostat	2021
VO_2/PMMA/Low E coated glass	Emissivity from 0.21 to 0.61 at transition temperature of 60 ℃	Indoor experiment	Self-adaptive radiative thermostat	2021
Cellulose glass	The long-wavelength infrared emissivity (ε_{LWIR}) for one side is as low as 0.3, to prevent the heat exchange, and the ε_{LWIR} of the other side is near unity (0.95)	Under direct solar irradiance	Smart window	2021

Table S3 UV protection property of different weaving methods

weaving methods	UPF	UVR%
Plain weave method	70.02	4.12
Square knitting method	60.13	4.18
Twill weave method	68.87	4.32
Satin weave method	72.09	3.92

References

1 Y. Wang, T. Wang, J. Liang, J. Wu, M. Yang, Y. Pan, C. Hou, C. Liu, C. Shen, G. Tao, X. Liu, *Mater. Horiz.* 2023, **10**, 5060-5070.

2 X. Wang, X. Liu, Z. Li, H. Zhang, Z. Yang, H. Zhou, T. Fan, *Adv. Funct. Mater.* 2019, **30**, 1907562.

3 J. Cao, H. Xu, X. Li, Y. Gu, *ACS Appl. Mater. Interfaces* 2023, **15**, 19480.

4 Y. N. Song, M. Q. Lei, J. Lei, Z. M. Li, *Mater. Today Energy* 2020, **18**, 100504.

5 C. Chen, X. Jia, X. Li, M. Shi, J. Hu, M. Song, S. Wu, H. Dai, X. Wang, H. Geng, *Chem. Eng. J.* 2023, **475**, 146307.

6 L. Cai, A. Y. Song, P. Wu, P.-C. Hsu, Y. Peng, J. Chen, C. Liu, P. B. Catrysse, Y. Liu, A. Yang, C. Zhou, C. Zhou, S. Fan, Y. Cui, *Nat. Commun.* 2017, **8**, 496.

7 Y.-N. Song, Y. Li, D.-X. Yan, J. Lei, Z.-M. Li, *Compos, Part A-Appl. S* 2020, **130**, 105738.

8 Y. Tian, X. Liu, Z. Wang, J. Li, Y. Mu, S. Zhou, F. Chen, M. L. Minus, G. Xiao, Y. Zheng, *Nano Energy* 2022, **96**, 107085.

9 S. P. Shaoning Zeng, Minyu Su, Zhuning Wang, Maoqi Wu, Xinhang Liu, Mingyue Chen, Yuanzhuo Xiang, Jiawei Wu, Manni Zhang, Qingqing Cen, Yuwei Tang, Xianheng Zhou, Zhiheng Huang, Rui Wang, Alitenai Tunuhe, Xiyu Sun, Zhigang Xia, Mingwei Tian, Min Chen, Xiao Ma, Lvyun Yang, Jun Zhou, Huamin Zhou, Qing Yang, Xin Li, Yaoguang Ma, Guangming Tao, *Science* 2021, **373**, 692.

10 X. Zhang, W. Yang, Z. Shao, Y. Li, Y. Su, Q. Zhang, C. Hou, H. Wang, *ACS Nano* 2022, **16**, 2188-2197.

11 Y. Sun, Y. Ji, M. Javed, X. Li, Z. Fan, Y. Wang, Z. Cai, B. Xu, *Advanced Materials Technologies* 2021, **7**, 2100803.

12 Y. Ji, Y. Sun, J. Muhammad, X. Li, Z. Liu, P. Tu, Y. Wang, Z. Cai, B. Xu, *Macromolecular Materials and Engineering* 2022, **307**, 2100795.

13 E. Pakdel, X. Wang, *Materials & Design* 2023, **231**, 112006.